Petrogenesis and geochemistry of fayalite and fluorite-bearing granite from the Assam Meghalaya Gneissic Complex, West Khasi Hills, Meghalaya, India: their implication towards Rodinia Supercontinent amalgamation

S. S. Sahoo*, Toshilila, J. M. Umlong, S. K. Bharti, J. K. Naik and T. Pal

Geological Survey of India, North Eastern Region, Shillong 793 006, India

The present study reports fayalite-bearing granite bodies from the Assam–Meghalaya Gneissic Complex of North East India. These are weakly peraluminous with high amounts of alkalis and meagre contents of magnesium, calcium, titanium and phosphorus. The chondrite normalized REE pattern is flat, having minor enrichment of HREE with negative europium anomaly suggesting their A-type character. The discrimination based on Rb, Y, Yb, Nb and Sc content indicates their generation due to melting of crustal components. Early crystallized fayalite and fluorite grains indicate that their emplacement in an extensional tectonic set-up most possibly represents the final stage of Rodinia Supercontinent amalgamation.

Keywords: Fayalite and fluorite granite, magmatism, mineral chemistry, petrography, supercontinent amalgamation.

FAYALITE and fluorite-bearing granites are volumetrically insignificant in nature[1–3] and are members of the most reduced anorogenic (A-type) granites[4], formed either by differentiation of mantle-derived mafic melts[5–8], partial melting of crustal components like metasediments[4,9], dehydrated lower crustalgranulites[9,10] or tonalites[5]. Low oxygen fugacity (fO_2) and low water activity (fH_2O) conditions favour crystallization of fayalite and late crystallization of hydrous mafic minerals such as Fe-rich amphibole and/or annite[11,12]. Fluorite is stable at high temperatures in peralkaline granites[13,14] and is commonly associated with A-type granites[9,15].

A-type granites rarely occur in continental and oceanic crust and occasionally in meteoritic and lunar rocks[15]. During the supercontinent assembly and break-up cycles, these granites are commonly emplaced in an extensional regime such as post-collisional extension, continental back-arc extension or within-plate settings[6,8,15–18]. A-type granites were initially characterized as metaluminous to peralkaline, high Fe/Mg, Zr + Nb + Ce + Y and Ga/Al and low CaO compared to metaluminous (I-type) and peraluminous (S-type) granites[7,9,19], and generally record high crystallization temperatures (830–1000°C)[5,10]. Later granitoids bearing a high Ga/Al ratio and the ferroan (high FeOt/MgO) nature like A-type granitoids were also included in this group[7,19,20]. As a consequence, some peraluminous granites bearing the above stated features have also been assigned as A-type granites[1,4,21–23].

Most of the fayalite-bearing granitoids are reported from the anorthosite–mangerite–charnockite–granite (AMCG) suite which was emplaced ~1 Ga during the final stages of assembly of the Rodinia Supercontinent[24] (Figure 1 *a*). The heat required for such extensive crustal melting has been attributed to mantle convection resulting from the thermal blanketing effect of the crust subsequent to supercontinent formation[24,25]. Only a few fayalite granitoids are known from Phanerozoic terrains, i.e. the anorogenic province of Corsica, France[26] and the Tibchi ring complex of Nigeria[11] in an active continental margin setting. In the Indian subcontinent, fayalite is reported from the Chimakurti pluton in the southern segment of the Eastern Ghats Belt of 1352 Ma, which documents a spatial and temporal association of both tholeiitic and alkaline endmembers of continental rift magmatism[18]. Fayalite granites of Gundlapalle, Gokanakonda in the Cuddapah intrusive province of Eastern Dharwar Craton (EDC) are differentiated products of gabbroic magma[27]. Ferrosyenites of Sivamalai, Tamil Nadu are crystallized from magma derived from the upper mantle source during 623 ± 21 Ma (Rb87/Sr86 age)[27].

The present study reports fayalite-granite bodies from the West Khasi Hills of Assam–Meghalaya Gneissic Complex (AMGC), which exhibit compositional features of A-type granites generated from melting of crustal rocks, most possibly emplaced during the final stage of Rodinia Supercontinent amalgamation.

Geology and tectonics

Proterozoic rocks of AMGC are the sole cratonic block in the northeastern part of the Indian peninsular shield.

*For correspondence. (e-mail: sidhartha.sahoo@gsi.gov.in)

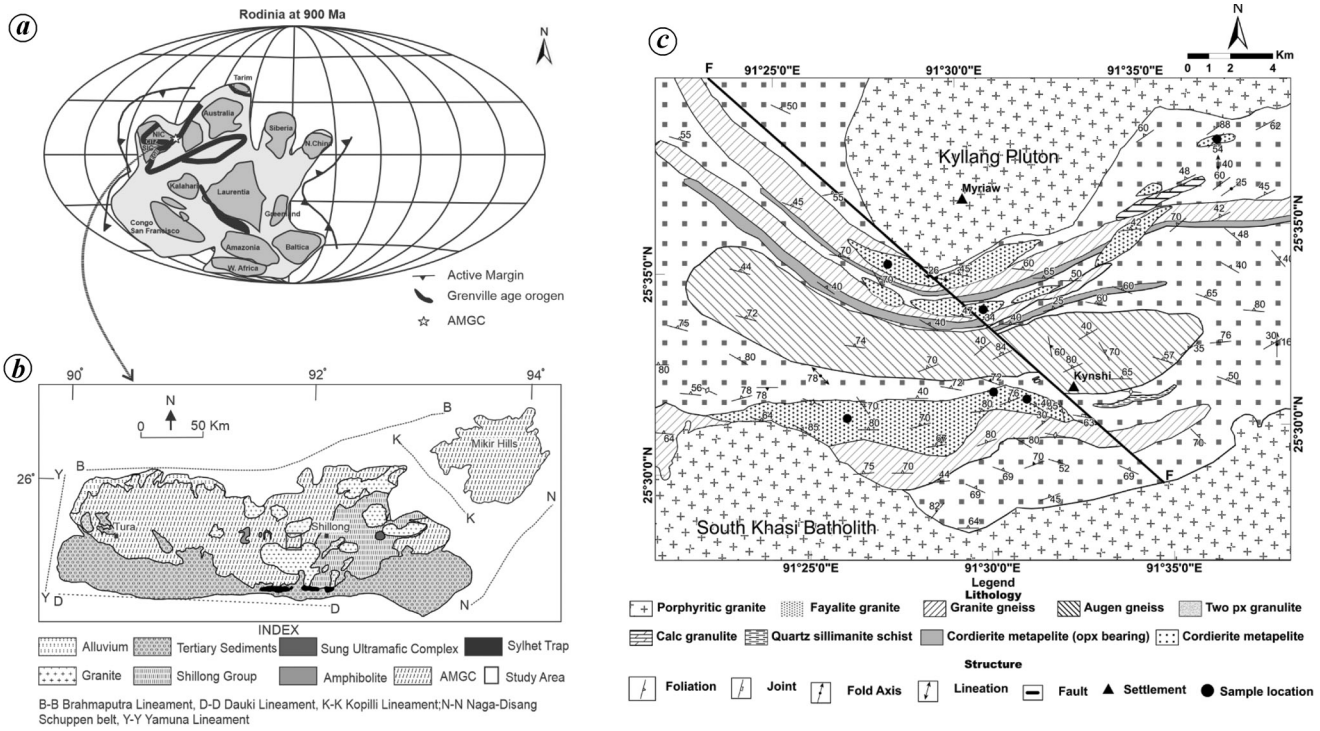

Figure 1. ***a***, Configuration of the Rodinia Supercontinent at *c*. 900 Ma showing assembled cratonic blocks and Grenville-age orogen (modified after Li *et al.*[68]). ***b***, Geological map of the Meghalaya Plateau[69]. ***c***, Geological map of the study area.

AMGC comprises of two horst-like structures, namely the Mikir massif in Assam and the Meghalaya massif in the west separated by SE-trending Kopili tectonic lineament[28–30]. The AMGC is bordered by Dauki Fault to the south[28,31], young folded Naga–Disang Schuppen Belt, Dhubri and Yamuna lineament to the west[32,33] and Brahmaputra lineament to the north[32,34,35]. These plateaus are considered to be an extension of the Chotnagpur Gneissic Complex (CGC)[30] (Figure 1 *a*) or the Eastern Ghats Mobile Belt (EGMB)[29] separated from the main Indian shield by Garo Rajmahal depression occupied by Quaternary alluvium of the Ganges and Brahmaputra rivers[36]. Recent studies substantiate this view by reporting the presence of Proterozoic basement gneisses below alluvium cover[37,38]. Gneissic rocks of AMGC have suffered upper amphibolite to granulite facies metamorphism[39,40]. It is postulated that AMGC is an extension of Central India Tectonic Zone (CITZ) since the Mesoproterozoic and is correlated to collision between the Southern Indian Block (SIB) and oceanic island arc to the north at *c*. 1.6 Ga, and a terminal collision between the SIB-arc composite and the Northern Indian Block (NIB) at *c*. 1 Ga that ultimately formed the Indian shield[41].

AMGC is exposed mostly in the central and northern parts of the Meghalaya massif covering the districts of West Garo Hills, East Garo Hills, West Khasi Hills and Ri Bhoi, and is composed mainly of paragneisses and intrusive granitoid gneisses (Figure 1 *b*). The para gneisses of > 1.7 Ga are the oldest components of AMGC[42] and have experienced multiple phases of deformation with the earliest being the gneissic layering of 1.1 Ga (refs 43–46). The AMGC experienced a major felsic magmatic episode during 1.6 Ga and 1.1 Ga (ref. 46). Yin *et al.*[46] correlated the early magmatic event to be arc-related and later to be a result of collision between NIB and SIB during the formation of Rodinia. Based on counter-clockwise *P–T–t* path recorded in the metasediments during 1.5 Ga, Chatterjee *et al.*[39] suggested an island arc set-up for AMGC.

Basement gneisses are unconformably overlain by the Shillong Group of metavolcano sedimentary sequence[47]. The gneissic complex and the Shillong Group of rocks are intruded by a number of post-tectonic Cambrian granite plutons[46,48]. The southern part of the plateau is covered by the Cretaceous Sylhet basalt and Tertiary shelf sediments.

Analytical methods

Petrography and geochemistry of the representative samples of fayalite granites were carried out. Major, minor oxides and trace elements (Ba, Ca, Cr, Cu, Ga, Nb, Ni, Pb, Rb, Sc, Sr, Th, V, Y, Zn, Zr) analyses were performed using an XRF spectrometer (PAN analytical Magix-2424) on pressed powder pellets placed in an aluminium cup over boric acid base. Rest of the trace and rare earth elements (REEs) were analysed by ICP-MS (Varian 820MS) at the Geological Survey of India (GSI), Kolkata. The composition of minerals was determined using an electron probe micro analyser (EPMA; CAMECA Sx10) at GSI, Kolkata. The operating conditions of EMPA were setup

Figure 2. Field photographs of different rocktypes exposed in the study area. ***a***, Migmatized Opx bearing cordierite metapelite with leucocratic Qtz ± Feldspar bands and melanocratic Bt + Opx + Gt + Sill + Opq bands. ***b***, Migmatized granite gneiss with garnet-rich leucosome. ***c***, Augen granite gneiss with augen shaped alkali felspar and aligned mafic grains defining gneissocity. ***d***, Massive fayalite granite showing buff colour and patches of green. ***e***, The contact between cordierite gneiss and fayalite granite (note the light colour upper right corner is fayalite granite, darker bottom left is cordierite metapelite and the intermediate part is garnetiferous/cordierite rich fayalite granite). ***f***, Enclave of cordierite gneiss in fayalite granite with diffused margin and occasional Bt rich margin. ***g***, Fayalite granite with clusters of coarse cordierite grains in the marginal part of the body. ***h***, Fayalite granite with clusters of coarse garnet grains in the marginal part of the body.

at 15 kV accelerating voltage, 12 nA beam current, and 1 μm electron beam size. All natural standards were used, except for Mn and Ti, for which synthetic standards were used for calibration. Mineral formulae and end-member calculations were done using Minpet 2.02 (ref. 49). Major silicate phases were classified according to the International Mineral Association (IMA) recommendations for the respective group of minerals.

Field relation

The study area is located near Kynshi village in the West Khasi Hills district, Meghalaya, about 60 km west of Shillong along NH 44E (Shillong–Nongstoin Road; Figure 1 *c*). The area comprises of E–W-folded rocks of cordierite-bearing metapelites of ~1.7 Ga (ref. 42), which are intruded by augen granite gneiss, granite gneiss, fayalite-bearing granite bodies and younger granite plutons of Cambrian age[48] (Figure 1 *c*). Cordierite-bearing metapelites are the most abundant litho component in the study area. They are usually composed of Cordierite (Crd), Garnet (Gt), Biotite (Bt), Sillimanite (Sill), Quartz (Qtz), Feldspar (Fsp) ± Orthopyroxene (Opx). The unit has been broadly divided into two assemblages with respect to the presence or absence of Opx. The Opx-bearing cordierite gneiss forms two narrow, easterly bands, whereas the other one is abundantly distributed all over the area. The units are extremely migmatized with leucomes developed parallel to the gneissocity. The leucosomes are composed of Qz ± Alkali Feldspar (Afs) and melanosomes of Bt + Gt + Crd + Opq ± Opx (Figure 2 *a*). At a few places porphyritic Grt and Opx are developed up to 2 cm in the leucosome part of the Opx-bearing association. The units have developed profuse Gt grains locally. Smaller bodies of calc granulite and Qtz-sill schist are marked with gradational contacts with the adjacent metapelites. Small basic

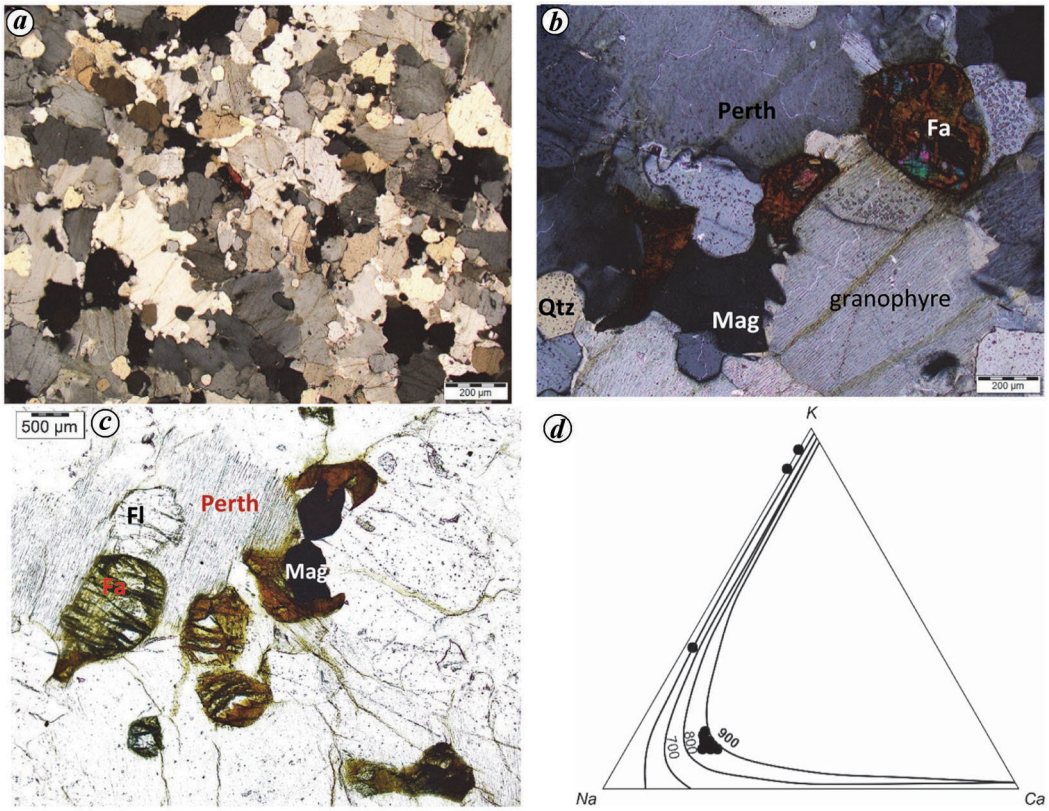

Figure 3 ***a–d.*** Photomicrographs. ***a***, Overall mineralogy and texture of fayalite and flourite-bearing granite. ***b***, Euhedral fayalite grain sharing sharp margin with granophyre and perthite grain. ***c***, Perthitic grain enclosing rounded fayalite grain and sharing margin with magnetite. ***d***, Mineral composition plot of feldspar in fayalite granite[70]. Note the feldspar falling in the ternary field indicating its hypersolvus crystallization.

granulite bodies have been demarcated within the cordierite gneiss. Granite gneisses are easterly disposed as narrow bands to the northern part of the Opx-bearing metapelite bands. The granite gneiss is composed of Qz + Fsp + Gt + Bt (Figure 2 *b*). The unit is Gt-rich and shows gradational contacts with the cordierite metapelites. The augen granite gneiss forms an E–W trending band of 3–4 km width with northerly, moderate-dipping gneissocity (Figure 2 *c*) and bears sharp contact with the adjacent lithounits. The augen granite gneiss is composed mainly of Qz + Fsp with variable quantities of Bt, amphibole (Amp) and magnetite (Mag), and is characterized by large ovoidal megacrysts of Fsp swerved around by the mafic minerals (Figure 1 *c*). Fayalite granite bodies occur as elliptical bodies within the metapelites and granite gneiss (varying up to 4–6 km along and 1 km across the width), which are mostly massive (Figure 2 *d*), and thus are younger than the metapelites, granite gneisses and augen gneiss (Figure 1 *c*). They share gradational margin with the adjacent metapelites and granite gneisses (Figure 2 *e*) and at places enclaves of metapelite are observed within these fayalite granites (Figure 2 *f*). The enclaves of cordierite gneiss usually share gradational margin with the Fayalite granite bodies and are occasionally bordered by a Bt-rich zone (Figure 2 *f*). The fayalite granite is coarse-grained, equigranular and buff to light grey to deep green in colour (Figure 2 *b*). It is composed of Fls and Qtz with minor amounts of Bt and occasionally Grt. The border between the cordierite gneiss and fayalite granite is occupied by a mixed zone, where coarse-grained cordierite or Gt form clusters in fayalite granite groundmass (Figure 2 *g* and *h*), whereas towards the core part, Gt grains are absent or rarely developed and cordierite is not observed. The southern and northern parts of the study area are occupied by prophyritic granite intrusive, i.e. South Khasi Batholith and Kyllang pluton respectively. The gneissic metasediments, augen granite gneiss and fayalite granite units are affected by the NW fault (*F–F* in Figure 1 *c*), which aborts against the South Khasi Batholith of Cambrian age[48]; thus, the fayalite granite bodies are older than the Cambrian plutons.

Petrography and mineral chemistry

Mineralogically, fayalite granites are composed of perthite and granophyric intergrowth of Qtz and Fsp, Qtz and minor amounts of plagioclase (Pl), Bt, Mag, Fa, Gt, nontronite, Fluorite (Fl), Apatite (Ap), zircon and thorite (Figure 3 *a*). Mesoperthite and granophyre constitute more

Table 1. Mineral chemistry and cation calculations for different phases of fayalite granite

Sample no.	1	2	3	4	5	6	7	8	9
Feldspar									
Na_2O	10.25	9.43	9.67	6.54	0.75	11.43	2.1	10.55	1.17
SiO_2	65.1	64.83	64	65.88	63.49	63.5	64.68	65.38	63.72
Al_2O_3	20.62	21.14	20.24	18.62	18.48	20.03	18	20.5	17.59
MgO	0	0.01	0.02	0	0	0	0.01	0.03	0.02
P_2O_5	0.01	0	0	0.02	0.01	0	0	0.03	0
K_2O	0.79	0.12	0.21	6.61	16.08	0.2	13.33	0.07	14.47
CaO	2	2.52	2.19	0.39	0	3.22	0	2.21	0
TiO_2	0.02	0	0	0	0	0	0	0	0
FeO	0.08	0.04	1.13	0.33	0.15	0.16	0	0.14	0.8
Cr_2O_3	0.02	0	0.05	0	0.03	0.03	0	0	0.01
MnO	0.12	0	0.13	0.01	0	0.04	0.02	0.03	0.04
ZnO	0.01	0	0	0.29	0	0	0.01	0	0.24
Total	99.02	98.09	97.64	98.69	98.99	98.61	98.15	98.94	98.06
Si	11.609	11.634	12.02	11.481	11.472	11.982	11.897	11.464	12.05
Al	4.33	4.296	3.908	4.516	4.489	3.988	4.078	4.259	3.949
Ti	0.003	0	0	0	0	0	0	0	0
Fe_2	0.012	0.021	0.126	0.006	0	0.05	0.024	0.024	0
Mn	0.018	0.005	0.006	0	0	0.002	0	0.006	0.003
Mg	0	0.008	0.006	0.003	0	0	0	0	0.003
Ca	0.382	0.421	0	0.552	0.501	0.076	0	0.623	0
Na	3.544	3.64	0.428	3.369	3.604	2.306	0.273	4.001	0.759
K	0.18	0.016	3.482	0.026	0.024	1.534	3.844	0.046	3.168
Cations	20.078	20.041	19.976	19.953	20.09	19.938	20.116	20.423	19.932
X	15.942	15.93	15.928	15.997	15.961	15.97	15.975	15.723	15.999
Z	4.136	4.111	4.048	3.956	4.129	3.968	4.141	4.7	3.933
Albite (%)	86.3	89.3	10.9	85.4	87.3	58.9	6.6	85.7	19.3
Anorthite (%)	9.3	10.3	0	14	12.1	1.9	0	13.3	0
Orthoclase (%)	4.4	0.4	89.1	0.7	0.6	39.2	93.4	1	80.7
Fayalite									
SiO_2	28.79	28.92	28.76	29.09	28.9	28.98	29.32		
Al_2O_3	0	0	0	0.02	0.03	0	0		
FeO	69.6	69.33	69.25	69.17	67.54	68.82	66.99		
MnO	1.64	1.67	1.55	1.5	1.33	1.3	1.23		
MgO	0.4	0.43	0.36	0.37	0.39	0.38	0.33		
Na_2O	0.03	0.07	0.11	0.06	0	0.04	0.07		
CaO	0	0.03	0.01	0.02	0.01	0.02	0		
K_2O	0.04	0.01	0	0.02	0.01	0	0		
Total	100.5	100.46	100.04	100.25	98.21	99.54	97.94		
Si	0.977	0.98	0.98	0.986	0.996	0.989	1.009		
Al	0	0	0	0.001	0.001	0	0		
Fe_2	1.976	1.966	1.973	1.961	1.947	1.964	1.927		
Mn	0.047	0.048	0.045	0.043	0.039	0.038	0.036		
Mg	0.02	0.022	0.018	0.019	0.02	0.019	0.017		
Ca	0	0.001	0	0.001	0	0.001	0		
Na	0.002	0.005	0.007	0.004	0	0.003	0.005		
K	0.002	0	0	0.001	0	0	0		
Cations	3.024	3.022	3.023	3.016	3.003	3.014	2.994		
X Fe = Fayalite	0.99	0.99	0.99	0.99	0.99	0.99	0.99		
X Mg = Forsterite	0.01	0.01	0.01	0.01	0.01	0.01	0.01		
Biotite									
Na_2O	0.19	0.1	0.16	0.03	0.1	0.08	0.05		
SiO_2	34.07	34.78	34.41	34.72	35.17	34.89	35.47		
Al_2O_3	12.54	12.67	12.46	12.45	12.75	12.62	13.12		
MgO	4.43	4.58	4.61	4.66	5.01	4.66	5.45		
P_2O_5	0	0	0	0.03	0	0	0		
K_2O	8.48	8.58	8.73	8.75	8.81	8.99	9.12		
TiO_2	4.19	4.04	4.22	3.98	3.54	3.76	3.89		
FeO	28.84	29.4	29.78	29.44	30.44	30.1	28.59		

(*Contd*)

Table 1. (*Contd*)

Sample no.	1	2	3	4	5	6	7	8	9
Cr_2O_3	0	0	0.02	0	0.04	0	0		
MnO	0.17	0	0.09	0.13	0.17	0.21	0.18		
ZnO	0	0.14	0.19	0.18	0.31	0	0		
Total	92.91	94.29	94.67	94.37	96.34	95.31	95.87		
Si	5.888	5.924	5.871	5.927	5.903	5.907	5.91		
AlIV	2.112	2.076	2.129	2.073	2.097	2.093	2.09		
AlVI	0.44	0.466	0.375	0.43	0.423	0.423	0.484		
Ti	0.545	0.518	0.542	0.511	0.447	0.479	0.488		
Fe_2	4.168	4.188	4.249	4.203	4.272	4.261	3.984		
Cr	0	0	0.003	0	0.005	0	0		
Mn	0.025	0	0.013	0.019	0.024	0.03	0.025		
Mg	1.141	1.163	1.173	1.186	1.253	1.176	1.354		
Na	0.064	0.033	0.053	0.01	0.033	0.026	0.016		
K	1.87	1.864	1.9	1.906	1.886	1.942	1.939		
Cations	16.253	16.232	16.308	16.265	16.343	16.337	16.29		
O	24	24	24	24	24	24	24		
X Fe = Annite	0.79	0.78	0.78	0.78	0.77	0.78	0.75		
X Mg = Phlogopite	0.21	0.22	0.22	0.22	0.23	0.22	0.25		

Table 2. Major Oxide concentration (wt%) of fayalite-granite and CIPW normative calculation

Sample no.	10210119	3191118	18120319	12080319	1270719	3270719	3070818
SiO_2	74.29	79.82	75.95	73.67	73.50	75.54	77.61
TiO_2	0.23	0.02	0.08	0.19	0.10	0.03	0.08
Al_2O_3	12.98	10.72	12.41	13.80	13.74	12.57	11.72
Fe_2O_3	1.80	0.41	1.01	1.58	1.72	1.15	0.67
MnO	0.02	0.01	0.03	0.03	0.04	0.05	0.01
MgO	0.24	0.02	0.11	0.20	0.18	0.10	0.05
CaO	1.04	0.68	0.55	0.52	0.97	0.68	0.66
Na_2O	4.41	3.34	3.45	3.25	3.18	3.42	3.07
K_2O	3.47	3.70	4.70	4.40	4.62	4.41	4.73
P_2O_5	0.03	0.01	0.03	0.04	0.03	0.02	0.02
LOI	0.93	0.86	0.86	1.42	1.25	1.17	0.91
Total	99.44	99.59	99.18	99.10	99.33	99.14	99.53
A/NK	1.18	1.13	1.15	1.37	1.34	1.21	1.15
A/CNK	1.01	1.00	1.05	1.25	1.15	1.08	1.03
Q	32.865	44.782	36.645	36.635	35.067	37.228	40.226
C	0.15	0.008	0.719	2.841	1.816	0.982	0.397
Or	20.507	21.866	27.776	26.003	27.303	26.062	27.953
Ab	37.316	28.262	29.193	27.501	26.908	28.939	25.977
An	4.964	3.308	2.533	2.318	4.616	3.243	3.144
Hy	0.598	0.05	0.274	0.498	0.448	0.249	0.125
Mt	0	0	0	0	0	0.076	0
Il	0.043	0.021	0.064	0.064	0.086	0.057	0.021
Hm	1.8	0.41	1.01	1.58	1.72	1.098	0.67
Ru	0.208	0.009	0.046	0.156	0.055	0	0.069
Ap	0.071	0.024	0.071	0.095	0.071	0.047	0.047
Total	98.521	98.74	98.331	97.691	98.091	97.98	98.63

than 90% by volume (Figure 3 *b*), which indicates that they have undergone extensive subsolvus changes. The mineral chemistry suggests Fsp grains to be ternary (Figure 3 *d* and Table 1 *a*). Exsolved Fsp occurs as anhedral grains, which tend to embay and enclose Fa (Figure 3 *c*), the Fe-end member of olivine ($Fa_{99}Fo_1$, Table 1) and Fl. Plagioclase is sparse and occurs as discrete subhedral grains. Qtz occurs occasionally as anhedral grains of irregular shape and mostly forms a granophyre texture. Annite, the Fe-end member of Bt makes up less than 2% of the mode (Table 1) and occurs as euhedral flakes in clusters forming symplectitic intergrowths with Qtz, sometimes surrounding Mag and as free euhedral grains. Fayalite constitutes less than 1% of the mode, is sparsely distributed and occurs as anhedral to subhedral grains up to 400 μm in diameter, which at places get replaced by clay mineral (nontronite). Finer Fa grains share sharp boundaries with larger perthitic Fsp, Qtz, Mag and Ilm (Figure 3 *b* and *c*).

Table 3. Trace and rare earth element concentration (ppm) of fayalite granites

Sample no.	10210119	3191118	18120319	12080319	1270719	3270719	3070818
Ba	835	64	277	914	217	47	45
Co	6	10	9	8	12	6	8
Cr	<15	44	27	20	<15	57	28
Cu	1	4	5	5	7	5	4
Ga	20	20	14	15	23	28	21
Nb	24	17	12	10	27	36	14
Ni	5	2	4	6	9	3	5
Pb	8	39	28	38	45	35	42
Rb	73	138	172	129	263	206	186
Sc	4	<3.5	<3.5	<3.5	<3.5	<3.5	<3.5
Sr	64	16	21	30	31	15	17
Th	27	13	24	15	49	25	19
V	<20	<20	<20	<20	<20	<20	<20
Y	98	63.00	58	47	205	150	32
Zn	18	34.00	26	45	36	20	23
Zr	286	124.00	102	180	151	103	162
Be	2.91	1.81	1.60	2.91	2.63	1	0.85
Ge	1.51	0.62	1.30	1.51	0.70	0.50	<0.50
Rb	62.45	140.92	165.71	62.45	213.40	171.25	163.17
Mo	1.03	1.23	2.37	1.03	2.95	3.55	4.94
Sn	9.52	<1.00	1.46	9.52	3.58	2.57	2.25
La	62.11	11.58	55.52	62.11	38.50	13.13	13.50
Ce	114.17	17.47	114.13	114.17	83.55	26.05	16.62
Pr	15.13	2.39	18.05	15.13	11.95	5.16	2.17
Nd	57.68	9.31	72.22	57.68	49.46	24.12	7.95
Sm	13.08	3.65	18.07	13.08	15.04	10.57	2.37
Eu	1.61	<0.50	0.63	1.61	0.75	<0.50	<0.50
Gd	14.45	5.33	16.38	14.45	17.06	12.99	2.87
Tb	2.79	1.39	2.66	2.79	4.14	3.56	0.68
Dy	19.94	11.80	15.58	19.94	33.61	28.19	5.44
Ho	4.26	2.80	3.00	4.26	7.90	6.13	1.30
Er	13.37	9.41	8.92	13.37	26.12	18.61	4.32
Tm	2.33	1.78	1.56	2.33	5.20	3.41	0.81
Yb	14.55	11.55	10.04	14.55	33.71	21.33	5.01
Lu	2.36	1.81	1.67	2.36	5.55	3.20	0.82
Hf	13.45	17.86	8.29	13.45	37.32	38.54	54.35
Ta	2.26	0.72	0.75	2.26	7.17	8.45	4.41
W	<0.50	<0.50	2.40	0.5	3.12	3.28	4.76
Th	26.78	18.06	25.54	26.78	65.67	42.36	19.71
U	3.40	6.33	3.84	3.4	11.05	12.11	3.75

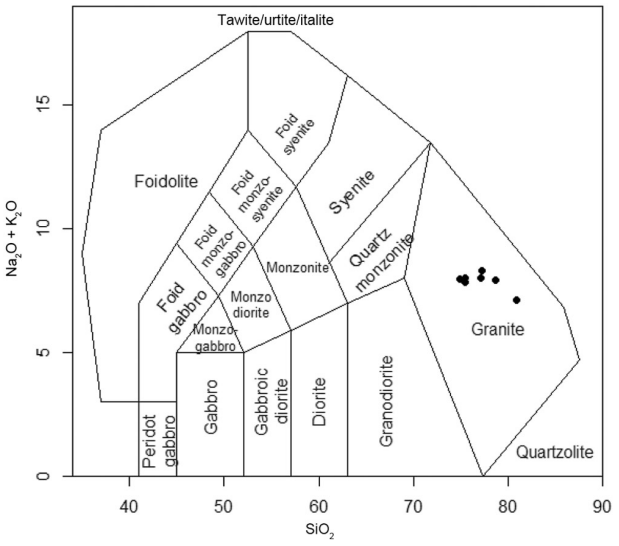

Figure 4. Geochemical classification of fayalite-bearing granite samples[71].

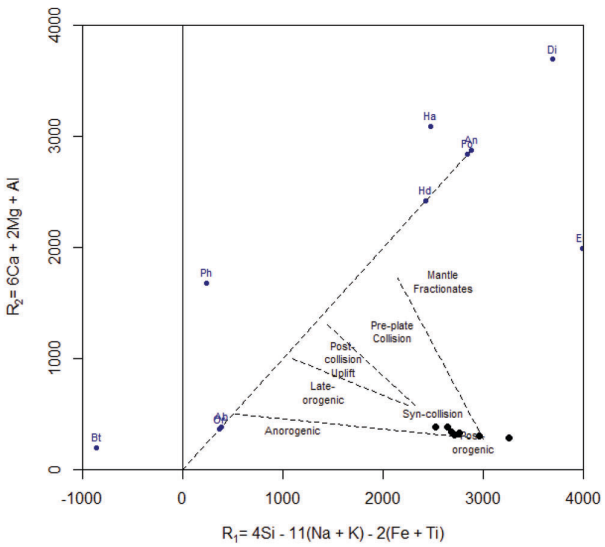

Figure 5. Geotectonic discrimination of fayalite-bearing granite samples[72].

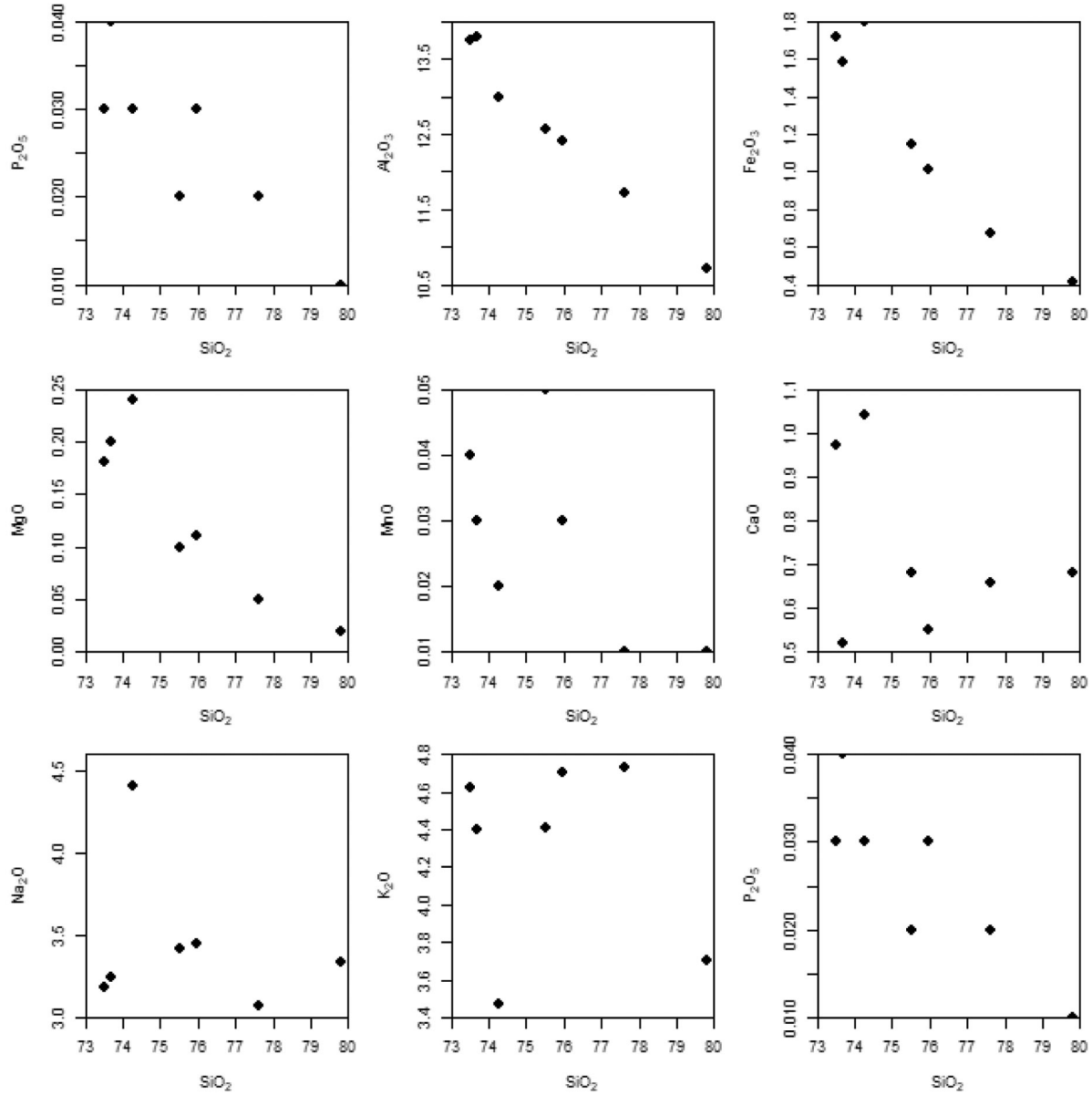

Figure 6. Harker's variation diagram of fayalite-bearing granite samples indicating magma differentiation during crystallization[73].

Exsolved Mag from Ilm grains is usually associated with Bt or Fa (secondary Mag replacing Fa; Figure 3 *b* and *c*) and as free euhedral grains. Zircon and apatite occur as minor accessory phases. Subhedral to anhedral Fl grains are poikilitically enclosed within Afs (Figure 3 *c*) and also occur as interstitial blebs.

Geochemistry

Seven representative samples of fayalite-bearing granite were analysed. The SiO_2 values were high and clustered between 73.30 wt% and 79.82 wt% (Table 2). The Al_2O_3 content was low to moderate, varying between 10.72 wt% and 13.80 wt%. The Fe_2O_3 content ranged from 0.41 wt% to 1.80 wt% and MgO from 0.41 wt% to 1.80 wt% with high Fe/Mg ratio varying between 8.70 and 15.54 and was ferroan-type. The CaO content was low varying from 0.52 wt% to 0.68 wt% (Table 2), with two samples having a higher content of 0.97 wt% and 1.04 wt%, with an average of 0.73 wt%. The samples had high content of Na_2O and K_2O, with Na_2O ranging between 3.07 wt% and 4.41 wt% and K_2O between 3.47 wt% and 4.73 wt% (Table 2). The $Na_2O + K_2O$ content ranged between 7.64 wt% and 8.15 wt%. The samples had K_2O/Na_2O usually >1, varying from 1.11 to 1.54, thus depicting the potash-rich character of the samples, except one sample having K_2O/Na_2O ratio of 0.78. The molar alumina saturation index $Al_2O_3/(CaO + Na_2O + K_2O)$ for the sample varied between 1.00 and 1.25, and $Al_2O_3/(Na_2O + K_2O)$ between 1.13 and 1.37; thus being weakly peraluminous.

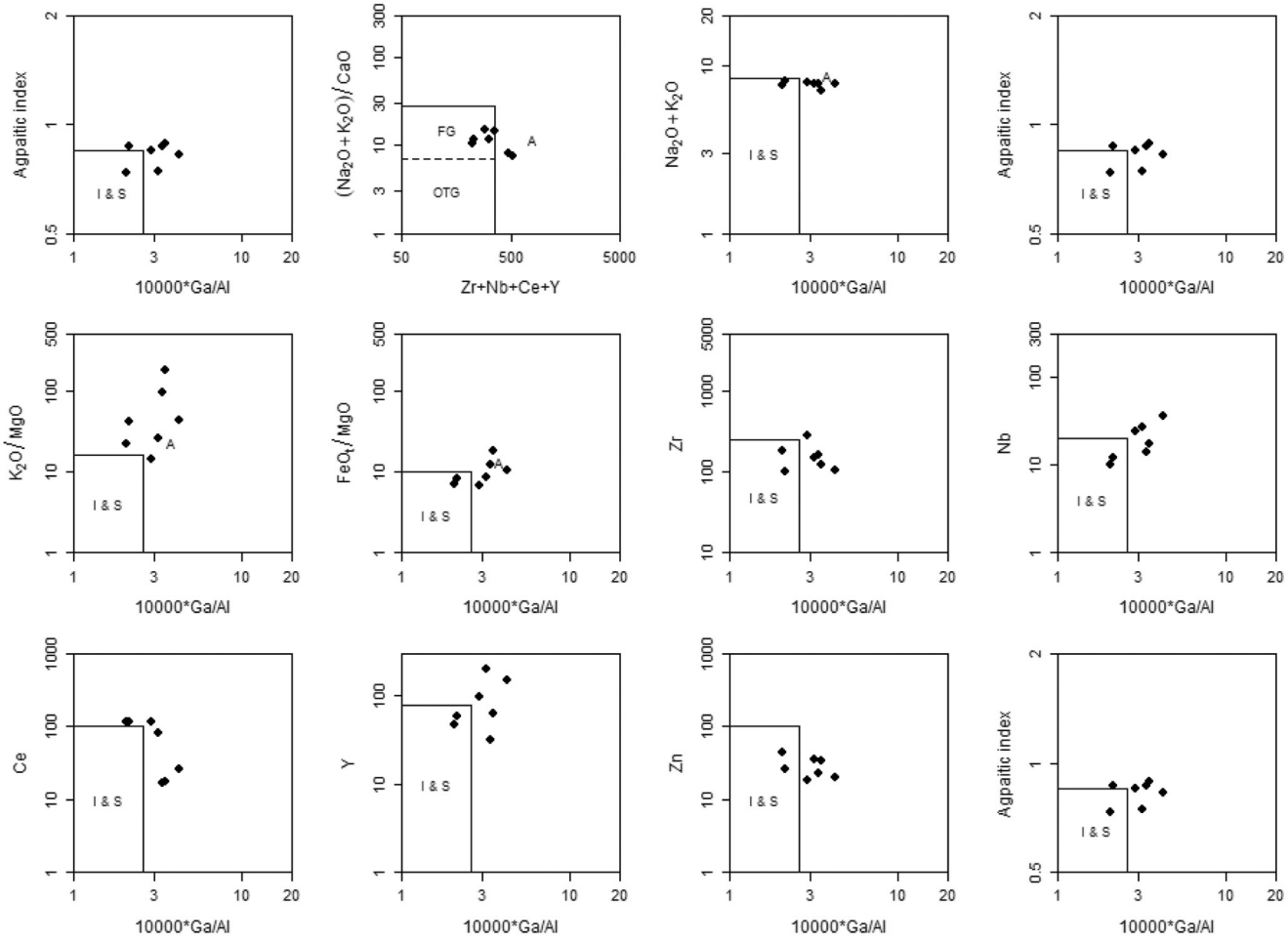

Figure 7. Geotectonic discrimination of fayalite-bearing granite samples[19].

The MnO ranged from 0.01 wt% to 0.05 wt%; TiO_2 from 0.02 wt% to 0.23 wt% and P_2O_5 from 0.01 wt% to 0.04 wt% (Table 2). In the TAS classification diagram, the samples plot within the granite field (Table 3 and Figure 4). In the multi-cationic R1–R2 tectonic discrimination plot, samples fall in a post-orogenic field (Figure 5). The major elements were plotted against SiO_2 on the Harker's variation diagram. They exhibited overall negative trends against SiO_2 except for K_2O and Na_2O, which showed positive trend (Figure 6). The samples were plotted in the tectonic discrimination plot of Whalen 1987 (Figure 7). In the plot of FeOt/MgO versus Zr + Nb + Ce + Y and $Na_2O + K_2O$/Cao versus Zr + Nb + Ce + Y, the samples were plotted at the margin of A-type granitoid field, whereas in Ga/Al versus $Na_2O + K_2O$ and $Na_2O + K_2O$/CaO, K_2O/MgO, Ce, all the samples were well within the A-type granitoid field. In the plot of Whalen[19] Ga/Al versus $Na_2O + K_2O$, FeO/MgO, Zr, Nb, Y, Zn and agpaitic index, majority of the samples showed A-type character, with one or two samples leaving close to the margin of A-type boundary. In terms of Rb, Y, Yb, Nb and Sc, the samples belonged to A_2 type of anorogenic granite, indicating their crustal source (Figure 8). The chondrite normalized REE showed relatively flat pattern with minor enrichment of HREE and significant negative europium anomalies which are considered to be the sole characteristics of A-type granites (Figure 9)[9,50]. HREE patterns of the samples were almost parallel, whereas LREE patterns showed two broad trends. One group of samples showed gentle to flat slope. The LREE slope patterns gradually decreased with increasing SiO_2 content, which is unusual for fractional crystallization processes. The unusual depletion of LREE in samples could be possibly due to early crystallization of LREE-rich accessory minerals like monazite or allanite[51].

Discussion and conclusion

Fayalite granites are analogous to charnockite with high FeO/(FeO + MgO) ratio[52]. At low to moderate pressure, systems with high FeO/(FeO + MgO) ratios, fayalite + quartz crystallizes instead of ferrosilite[53–56]. However, only high FeO/(FeO + MgO) ratio in the host rock does not

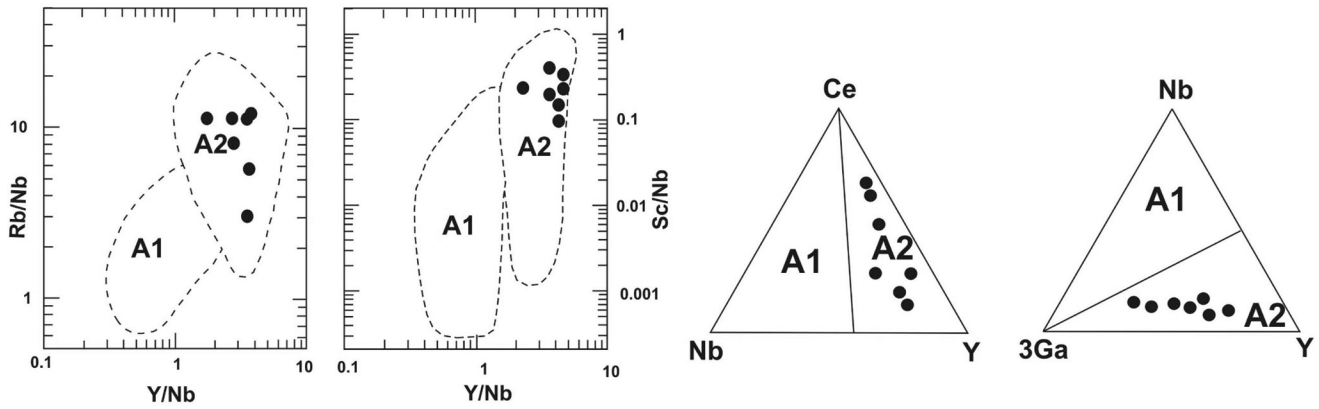

Figure 8. Rb/Nb versus Y/Nb and Sc/Nb versus Y/Nb, and triangular plots for A-type granitoid suites to distinguish between A1 and A2 groups[16]. Note samples of fayalite-granite falling in the A2 field, indicating their crustal origin.

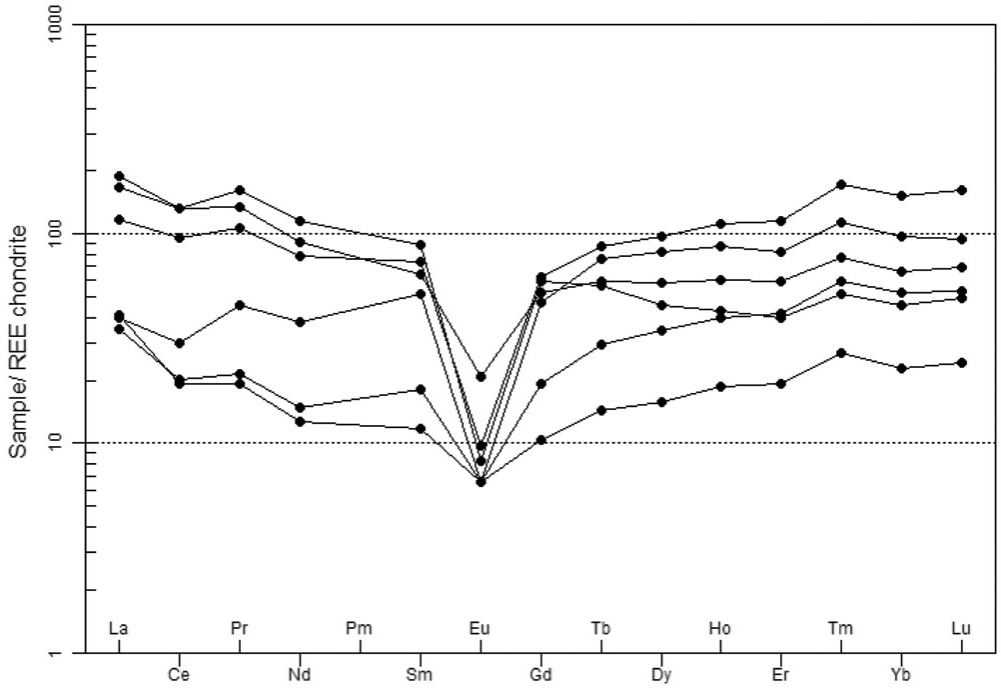

Figure 9. Chondrite normalized spider plot of fayalite-bearing granite samples[74].

ensure fayalite stabilization in anhydrous ferromagnesian silicate. A low Ti content and low oxygen fugacity inhibit crystallization of significant amounts of ilmenite and magnetite respectively, favouring crystallization of fayalite, provided the initial FeO/(FeO + MgO) ratio and T–Pr–PH_2O conditions are appropriate. Analyses of fayalite granite presented here show FeO/(FeO + MgO) to range from 0.87 to 0.94, with a mean value of 0.90, while TiO_2 content is very low, i.e. 0.08–0.23 wt% with a mean value of 0.10 wt%. A variety of fluoride minerals can precipitate from F-bearing aluminosilicate melts, including fluorite, cryolite, villiaumite and fluortopaz. From thermodynamic calculations and observed parageneses, Stormer and Carmichael[57] concluded that fluorite crystallizes in magmas that are not unusually poor in calcium, whereas cryolite should be the stable fluoride in Ca-poor, silica-oversaturated magmas. However, fluorite has also been reported in several Ca-poor (CaO < 0.5 wt%) granites[58,59]. Fluorite crystallizes within high-temperature, low-pressure, moderate fO_2, sub-aluminous felsic rocks[60,61]. In the studied samples, Fa and Fl grains embedded within the perthites indicate their early crystallization from melt and the low pressure condition during their emplacement. The occurrence of ilmenite lamellae in magnetite indicates oxidation and exsolution of the original ulvospinel component from the primary titanomagnetite phase during cooling; a phenomenon common in titanomagnetites of plutonic rocks. Presence of annite in interstitial spaces and sympletic

growth of annite and quartz indicate their late-stage crystallization. Fine grain size, allotriomorphic texture and profuse development of perthites and granophyres indicate rapid cooling of the melt and subsolvous changes. The presence of ternary Fsp, and profuse development of perthites and granophyres suggest hypersolvus crystallization at a higher temperature of about 900°C (refs 62, 63). The early crystallized Fa and Fl embedded within the ternary perthites thus indicate crystallization of melt in a low-pressure and high-temperature condition at shallow crustal depths[60,64,65]. The A1 granites represent mantle differentiates emplaced during intraplate rifting, usually with abundant coeval mafic rocks, or as the result of inferred plume or hotspot activity. The A2 granites represent a much broader range of environments and include post-collisional granites and those that were emplaced at the end of a long period of apparently high heat flow and granitic magmatism[16]. Unlike I- and S-type granites, A-type granites rarely contain deformational fabric. They occur in anorogenic (i.e. unrelated to orogenesis in space or time) and continental rift settings, or in the orogenic cycle they post-date the development of convergent strain (usually by less than 30 Ma)[12]. The undeformed studied rocks of A2-type are intimately associated with the metasediments, and no bodies of mafic or intermediate composition are found. For the formation of these rocks, a much higher than normal crustal temperature at low pressure conditions is required. Thus, an additional heat source due to asthenospheric upwelling and/or basaltic underplating is speculated for their genesis[66,67].

Bidyananda and Deomurari[43] carried out U–Pb zircon geochronology of the metapelitic gneisses of AMGC and suggested >1.98 Ga age for the metasediments which have undergone metamorphism during 1.67–1.98 Ga. Metamorphic age of ~1.7 Ga for granitoid gneiss was reported by Ghosh *et al.*[68] for the Patharkhang area. Chatterjee *et al.*[39] carried out monazite geochronology of metasediments from the Garo-Goalpara area from the western part of AMGC, which yielded 1621 ± 16 Ma, metamorphism along the counterclockwise *P–T–t* path with peak metamorphism at 850°C/7.5 kb and suggested the island arc set-up for AMGC. Bidyananda and Deomurari[42] and Yin *et al.*[46] obtained ages of granite intrusion at ~1.6 Ga and ~1.1 Ga respectively, in AMGC and related the ~1.1 Ga event to collision between India–Antarctica and Australia–South Tibet during the formation of Rodinia Supercontinent. Yin *et al.*[46] also demonstrated the age of formation of gneissic foliation to be ~1.1 Ga by dating adjacent units of undeformed granite vein of 1084 ± 19 Ma and deformed granites of 1110 ± 15 Ma. Bidyananda and Deomurari[42] have suggested extensive charnockite magmatism during 1.0–1.3 Ga in AMGC. The Fa granite bodies lying adjacent to the granitoid gneisses are undeformed and thus younger than 1.1 Ga. The northern and southern parts of the study area are occupied by plutons of the Cambrian age. The gneisses and fayalite granite bodies are affected by the NW fault in the central part of the study area. Thus, the bodies are older than the undeformed granites of South Khasi Batholiths of 516 ± 9.0 Ma age[20].

Except for a few, fayalite-bearing granitoids are mostly reported from the AMCG suite, which was emplaced at ~1 Ga during the final stages of assembling the Rodinia Supercontinent[24]. The heat required for such an extensive crustal melting has been attributed to mantle convection resulting from the thermal blanketing effect of the crust subsequent to supercontinent formation[24,25]. The bodies being situated in the grenvillian orogenic belt and emplaced in an extensional tectonic set-up between 1.1 and 5.16 Ga thus most probably represent the magmatism during the final stage of Rodinia Supercontinent amalgamation.

1. Stephenson, N. C. N. and Hensel, H. D., A precambrian fayalite granite from the south coast of Western Australia. *Lithos*, 1978, **11**, 209–218.
2. Vasquez, P., Glodny, J., Franz, G., Romer, R. L. and Gerdes, A., Origin of fayalite granitoids: new insights from the Cobquecura Pluton, Chile, and its metapelitic xenoliths. *Lithos*, 2009, **110**, 181–198.
3. Frost, B. R. and Frost, C. D., On charnockites. *Gondwana Res*., 2008, **13**, 30–44.
4. Huang, H. Q., Li, X. H., Li, W. X. and Li, Z. X., Formation of high $\delta^{18}O$ fayalite-bearing A-type granite by high temperature melting of granulitic metasedimentary rocks, southern China. *Geology*, 2011, **39**, 903–906.
5. Creaser, R. A., Price, R. C. and Wormald, R. J., A-type granites revisited: assessment of a residual-source model. *Geology*, 1991, **19**, 163–166.
6. Frost, C. D. and Frost, R. B., Reduced rapakivi-type granites: the tholeiite connection. *Geology*, 1997, **25**, 647.
7. Loiselle, M. C. and Wones, D. R., Characteristics and origin of anorogenic granites. *Geol. Soc. Am.*, 1979, **11**, 468.
8. Frost, C.., Frost, B.., Bell, J. and Chamberlain, K., The relationship between A-type granites and residual magmas from anorthosite: evidence from the northern Sherman batholith, Laramie Mountains, Wyoming, USA. *Precambrian Res*., 2002, **119**, 45–71.
9. Collins, W. J., Beams, S. D., White, A. J. R. and Chappell, B. W., Nature and origin of A-type granites with particular reference to southeastern Australia. *Contrib. Miner. Petrol*., 1982, **80**, 189–200.
10. Clemens, J. D., Holloway, J. R. and White, A. J. R., Origin of an A-type granite: experimental constraints. *Am. Mineral*., 1986, **71**, 317–324.
11. Mucke, A., Fayalite, pyroxene, amphibole, annite and their decay products in mafic clots within Younger Granites of Nigeria: petrography, mineral chemistry and genetic implications. *J. Afr. Earth Sci*., 2003, **36**, 55–71.
12. Turner, S. P., Foden, J. D. and Morrison, R. S., Derivation of some A-type magmas by fractionation of basaltic magma: an example from the Padthaway Ridge, South Australia. *Lithos*, 1992, **28**, 151–179.
13. Scaillet, B. and Macdonald, R., Fluorite stability in silicic magmas. *Contrib. Mineral. Petrol*., 2004, **147**, 319–329.
14. Scaillet, B. and MacDonald, R., Phase relations of peralkaline silicic magmas and petrogenetic implications. *J. Petrol*., 2001, **42**, 825–845.
15. Bonin, B., A-type granites and related rocks: evolution of a concept, problems and prospects. *Lithos*, 2007, **97**, 1–29.
16. Eby, G. N., Chemical subdivision of the A-type granitoids: petrogenetic and tectonic implications. *Geology*, 1992, **20**, 641.

17. Njonfang, E. and Moreau, C., The mafic mineralogy of the Pandé massif, Tikar plain, Cameroon: implications for a peralkaline affinity and emplacement from highly evolved alkaline magma. *Mineral. Mag*., 2000, **64**, 525–537.
18. Kumar, V. K., Frost, C. D., Frost, B. R. and Chamberlain, K. R., The Chimakurti, Errakonda, and Uppalapadu plutons, Eastern Ghats Belt, India: an unusual association of tholeiitic and alkaline magmatism. *Lithos*, 2007, **97**, 30–57.
19. Whalen, J. B., Currie, K. L. and Chappell, B. W., A-type granites: geochemical characteristics, discrimination and petrogenesis. *Contrib. Miner. Petrol*., 1987, **95**, 407–419.
20. Eby, G. N., The A-type granitoids: a review of their occurrence and chemical characteristics and speculations on their petrogenesis. *Lithos*, 1990, **26**, 115–134.
21. Gao, P., Garcia, A. M., Chen, Y. X. and Zhao, Z. F., Origin of peraluminous A-type granites from appropriate sources at moderate to low pressures and high temperatures. *Lithos*, 2020, **352**.
22. Dahlquist, J. A., Alasino, P. H. and Bello, C., Devonian F-rich peraluminous A-type magmatism in the proto-Andean foreland (Sierras Pampeanas, Argentina): geochemical constraints and petrogenesis from the western-central region of the Achala batholith. *Mineral. Petrol*., 2014, **108**, 391–417.
23. King, P. L., White, A. J. R., Chappell, B. W. and Allen, C. M., Characterization and origin of aluminous A-type granites from the Lachlan Fold Belt, southeastern Australia. *J. Petrol*., 1997, **38**, 371–391.
24. Winter, J. D., Subduction related igneous activity, Part I: Island Arcs. In *Principles of Igneous and Metamorphic Petrology*, Pearson Publ., Seventh im, 2018, pp. 339–368.
25. McLelland, J. M., Selleck, B. W., Hamilton, M. A. and Bickford, M. E., Late- to post-tectonic setting of some major proterozoic anorthosite–mangerite–charnockite–granite (AMCG) suites. *Can. Mineral*., 2010, **48**, 729–750.
26. Poitrasson, F., Duthou, J. L. and Pin, C., The relationship between petrology and Nd isotopes as evidence for contrasting anorogenic granite genesis: example of the Corsican Province (SE France). *J. Petrol*., 1995, **36**, 1251–1274.
27. Rao, T. V. S., Narayana, B. L. and Gopalan, K., Rb–Sr age of the Sivamalai alkaline complex, Tamil Nadu. *Earth Planet. Sci*., 1994, **103**, 425–437.
28. Evans, P., The tectonic framework of Assam. *J. Geol. Soc. India*, 1964, **5**, 80–96.
29. Crawford, R., Indo-Antarctica, Gondwanaland, and the distortion of a granulite belt. *Tectonophysics*, 1974, **22**, 141–157.
30. Desikacher, S. V., A review of the tectonic and geological history of eastern India in terms of plate tectonic theory. *J. Geol. Soc. India*, 1974, **15**, 137–149.
31. Biswas, S. and Grasemann, B., Quantitative morphotectonics of the southern Shillong Plateau (Bangladesh/India). *Aust. J. Earth Sci*., 2005, **97**, 82–83.
32. Gupta, R. P. and Sen, A. K., Imprints of ninety–east Ridge in the Shillong Plateau, Indian Shield. *Tectonophysics*, 1988, **154**, 335–341.
33. Nakata, T., Active faults of the Himalaya of India and Nepal. *Geol. Soc. Am. Spec. Pap.*, 1989, **232**, 243–264.
34. Rajendran, C. P., Rajendran, K., Duarah, B. P., Baruah, S. and Earnest, A., Interpreting the style of faulting and paleoseismicity associated with the 1897 Shillong, northeast India, earthquake: implications for regional tectonism. *Tectonics*, 2004, **23**, 1–12; doi:10.1029/2003TC001605.
35. Clark, M. K. and Bilham, R., Miocene rise of the Shillong Plateau and the beginning of the end for the Eastern Himalaya. *Earth Planet. Sci. Lett*., 2008, **269**, 337–351.
36. Eremenco, N. A. *et al.*, Tectonic map of India – Principles of preparation. *Bull. ONGC*, 1969, **6**, 1–111.
37. Ameen, S. M. M. *et al.*, Paleoproterozoic granitoids in the basement of Bangladesh: a piece of the Indian Shield or an exotic fragment of the Gondwana jigsaw. *Gondwana Res*., 2007, **12**, 380–387.
38. Hossain, I., Tsunogae, T., Rajesh, H., Chen, B. and Arakawa, Y., Palaeoproterozoic U–Pb SHRIMP zircon age from basement rocks in Bangladesh: a possible remnant of the Columbia Supercontinent. *Geoscience*, 2007, **339**, 979–986.
39. Chatterjee, N., Mazumdar, A. C., Bhattacharya, A. and Saikia, R. R., Mesoproterozoic granulites of the Shillong–Meghalaya Plateau: evidence of westward continuation of the Prydz Bay Pan-African suture into northeastern India. *Precambrian Res*., 2007, **152**, 1–26.
40. Lal, R. K., Ackerman, D., Seifert, F. and S. K. H., Chemographic relationships in sapphirine-bearing rocks from Sonapahar, Assam, India. *Contrib. Mineral. Petrol*., 1978, **67**, 169–187.
41. Chatterjee, N., Constraints from monazite and xenotime growth modelling in the MnCKFMASH–PYCe system on the *P–T* path of a metapelite from Shillong–Meghalaya Plateau: implications for the Indian shield assembly. *J. Metamorph. Geol*., 2017, **35**, 393–412.
42. Bidyananda, M. and Deomurari, M. P., Geochronological constraints on the evolution of Meghalaya massif, northeastern India: an ion microprobe study. *Curr. Sci*., 2007, **93**, 1620–1623.
43. Ahmed, M., Depositional environment of the basal conglomerate of the Barapani Formation, Shillong Group, Khasi Hills, Meghalaya. *Geol. Miner. Metall. Soc., India*, 1983, **55**, 62–68.
44. Nandy, D. R., Geodynamics of the Northeastern India and the adjoining Region. *ACB. Publ.*, 2001, **209**.
45. Majumdar, D. and Dutta, P., Geodynamic evolution of a Pan-African granitoid of extended Dizo Valley in Karbi Hills, NE India: evidence from geochemistry and isotope geology. *J. Asian Earth Sci*., 2016, **117**, 256–268.
46. Yin, A. *et al.*, Geologic correlation of the Himalayan orogen and Indian craton: Part 1. Structural geology, U-Pb zircon geochronology, and tectonic evolution of the Shillong Plateau and its neighboring regions in NE India. *Bull. Geol. Soc. Am*., 2010, **122**, 336–359.
47. Naik, R. R. *et al.*, Characteristics of Mesoproterozoic felsic metavolcanics from the Shillong Group of rocks, Meghalaya, North East India. *Curr. Sci*., 2020, **118**, 1123–1128.
48. Kumar, S. *et al.*, Contribution of Columbia and Gondwana Supercontinent assembly- and growth-related magmatism in the evolution of the Meghalaya Plateau and the Mikir Hills, Northeast India: constraints from U–Pb SHRIMP zircon geochronology and geochemistry. *Lithos*, 2017, **277**, 356–375.
49. Richard, L. R., Mineralogical and petrological data processing system, version 2.02. MinPet Geological Software, Québec, Canada, 1995.
50. Jackson, N. J., Walsh, J. N. and Pegram, E., Geology, geochemistry and petrogenesis of late Precambrian granitoids in the Central Hijaz Region of the Arabian Shield. *Contrib. Miner. Petrol*., 1984, **87**, 205–219.
51. Miller, C. F. and Mittlefehldt, D. W., Depletion of light rare-earth elements in felsic magmas. *Geology*, 1982, **10**, 129–133.
52. Waard, D., The occurrence of charnockite in the Adirondacks: a note on the origin and defination of charnockite. *Am. J. Sci.*, 1969, **267**(8), 983–987.
53. Bowen, N. L. and Schairer, J. F., The system MgO–FeO–SiO_2. *Am. J. Sci*., 1935, **229**, 151–217.
54. Lindsley, D. H. and Munoz, J. L., Subsolidus relation along the join hedenbergite–ferrosilite. *Am. J. Sci*., 1969, **267**, 295–324.
55. Smith, D., Stability of the assemblage iron-rich orthopyroxene–olivine–quartz. *Am. J. Sci*., 1971, **271**, 370–382.
56. Smith, D., Stability of iron-rich pyroxene in the system $CaSiO_3$–$FeSiO_3$ – $MgSiO_3$. *Am. Mineral*., 1972, **57**, 1413–1428.
57. Stormer, J. C. and Carmichael, I. S. E., Villiaumite and the occurrence of fluoride minerals in igneous rocks. *Am. Mineral*, 1970, **55**, 126–134.

58. Charoy, B. and Raimbault, L., Zr-, Th- and REE-rich biotite differentiates in the A-type granite pluton of Suzhou (Eastern China): the key role of fluorine. *J. Petrol*., 1994, **35**, 919–962.
59. Haapala, I., Magmatic and postmagmatic processes in tin-mineralized granites: topaz-bearing leucogranite in the Eurajoki Rapakivi Granite Stock, Finland. *J. Petrol*., 1997, **38**, 1645–1659.
60. Price, J. D., Hogan, J. P., Gilbert, M. C., London, D. and Morgan VI, G. B., Experimental study of titanite–fluorite equilibria in the A-type Mount Scott granite: implications for assessing F contents of felsic magma. *Geology*, 1999, **27**, 951–954.
61. Weidner, J. R. and Martin, R. F., Phase equilibria of a fluorine-rich leucogranite from the St. Austell pluton, Cornwall. *Geochim. Cosmochim. Acta*, 1987, **51**, 1591–1597.
62. Fuhrman, M. L. and Lindsley, D. H., Ternary feldspar modeling and thermometry. *Am. Mineral*., 1988, **73**, 201–215.
63. Nekvasil, H., Ternary feldspar/melt equilibria: a review. In *Feldspars and their Reactions* (ed. Parsons, I.), Springer, 1994, vol. 421, pp. 195–219.
64. Loury, C. *et al*., Permian charnockites in the Pobeda area: implications for Tarim mantle plume activity and HT metamorphism in the South Tien Shan range. *Lithos*, 2018, **304**–**307**, 135–154.
65. Harrison, T. N., Parsons, I. and Brown, P. E., Mineralogical evolution of fayalite-bearing rapakivi granites from the Prins Christians Sund pluton, South Greenland. *Mineral. Mag*., 1990, **54**, 57–66.
66. Bea, F., The sources of energy for crustal melting and the geochemistry of heat-producing elements. *Lithos*, 2012, **153**, 278–291.
67. Clemens, J. D., Melting of the continental crust: fluid regimes, melting reactions, and source-rock fertility. In *Evolution and Differentiation of the Continental Crust* (eds Brown, M. and Rushmer, T.), Cambridge University Press, Cambridge, UK, 2006, pp. 297–331.
68. Li, Z. X. *et al.*, Assembly, configuration, and break-up history of Rodinia: a synthesis. *Precambrian Res*., 2008, **160**, 179–210.
69. GSI, *Geology and Mineral Resources of Meghalaya*, Misc. Pub. No 30 part IV, 2, 2009.
70. Elkins, L. T. and Grove, T. L., Ternary feldspar experiments and thermodynamic models. *Am. Mineral*., 1990, **75**, 544–559.
71. Middlemost, E. A. K., Naming materials in the magma/igneous rock system. *Earth Sci. Rev*., 1994, **37**, 215–224.
72. Batchelor, R. A. and Bowden, P., Petrogenetic interpretation of granitoid rock series using multicationic parameters. *Chem. Geol*., 1985, **48**, 43–55.
73. Harker, A., *The Natural History of Igneous Rocks*, Methuen & Co, 1909, p. 384.
74. Nakamura, N., Determination of REE, Ba, Fe, Mg, Na and K in carbonaceous and ordinary chondrites. *Geochim. Cosmochim. Acta*, 1974, **38**, 757–775.

Received 8 September 2020; revised accepted 25 February 2022

doi: 10.18520/cs/v122/i10/1161-1173